Maximum directivity of flanged open-ended waveguides

Hao Dong, Jean-Baptiste Doc, Simon Félix

JASA ARTICLE

Maximum directivity of flanged open-ended waveguides

Hao Dong,[1,a] Jean-Baptiste Doc,[2] and Simon Félix[1]

[1]*Laboratoire d'Acoustique de l'Université du Mans (LAUM), UMR 6613, Institut d'Acoustique Graduate School (IA-GS), CNRS, Le Mans Université, Avenue Olivier Messiaen, 72085 Le Mans, France*

[2]*Laboratoire de Mécanique des Structures et des Systèmes Couplés, Conservatoire National des Arts et Métiers, 2 Rue Conté, 75003 Paris, France*

ABSTRACT:

Directional beams have extensive applications in communication and sound reproduction. This paper investigates the theoretical maximum directivity of infinitely flanged open-ended waveguides and the radiation pattern synthesis. We derive a rigorous solution for the maximum directivity factor of a flanged aperture with arbitrary shape by projecting its surface velocity on the waveguide modes, enabling the creation of a directional beam in any desired direction. We present case studies for a three-dimensional circular waveguide and a bidimensional waveguide. The theoretical beam that is obtained in a subspace spanned by all the propagating modes can then be synthesized by a group of incident modes or a point-source array within the waveguide. The optimality of the beam is demonstrated by comparing it with Gaussian shaded modes radiated from the waveguide. If the evanescent modes are taken into account, the maximum directivity factor increases with considerable loss to the radiation efficiency. Nevertheless, the optimum aperture velocity dominated by its evanescent components is capable of precise beam steering in extreme directions and could be useful for designing material-filled horns. Our work provides benchmark directivity factors and patterns for the practical design of horn antennas. In addition, we present a generalized form of Bouwkamp's impedance theorem. © *2023 Acoustical Society of America*. https://doi.org/10.1121/10.0020052

(Received 31 March 2023; revised 13 June 2023; accepted 15 June 2023; published online 10 July 2023)

[Editor: Lixi Huang] Pages: 115–125

I. INTRODUCTION

Directional sound radiation is desired in applications such as underwater acoustic communication, targeted warning, and public address. Various active and passive approaches have been developed for generating directional beams, e.g., loudspeaker arrays[1,2] based on the linear modulation of relative source strengths, parametric acoustic arrays[3] exploiting the nonlinear interactions, acoustic horns,[4] metasurfaces,[5] and metamaterial lenses.[6] As the directivity factor is a common metric to measure the directivity, directional beams can be achieved by performing numerical optimization with respect to it.[7] In addition, rigorous and closed-form solutions of the maximum directivity factor have been studied for acoustic line source arrays[8] and spherical arrays.[9] In this paper, we conduct a fundamental investigation into the maximum directivity of a flanged aperture by modal decomposition, followed by a study on the synthesis of the optimal patterns via guided waves.

The subject of sound radiation from open-ended waveguides has been studied intensively, e.g., rigorous analysis of end reflection and far-field diffraction from unflanged[10–14] and infinitely flanged waveguides,[15,16] and a semi-analytical approach to the generalized radiation impedances of waveguides with arbitrary wall thickness.[17] For flanged waveguides, Rayleigh's diffraction theory[18] has also been extensively used for the analysis of modal radiation efficiency,[19] generalized radiation impedances and reflection coefficients,[20,21] and far-field directivity patterns.[14,22] Other than these forward analyses of radiation, inverse design of waveguides for super-directivity is of great practical importance, e.g., metamaterial lens antenna.[23] However, to the best of our knowledge, the theoretical maximum directivity factor of an acoustic aperture is still an open question. The lack of this maximum value and a benchmark directivity pattern would challenge the design and assessment of super-directive waveguides. The axial directivity is usually benchmarked against a piston vibrator,[24] but it is questionable whether a uniform velocity distribution is the optimum solution.

Polo-López *et al.*[25] have studied the directivity maximization of an electromagnetic aperture antenna, to which our work can be analogous. In their study, the physical optics approximation (POA)[26] is implicitly used, which neglects the scattering of incident fields on the aperture and assumes the fields diffracted into the sideline directions vanish. As the antenna engineering community is mainly interested in moderate- to high-gain designs, the POA is often applied with success.[26] In acoustics, however, the low-frequency behavior is deemed highly significant, and it is, thus, essential to develop a rigorous theory applicable to all frequencies. They performed maximization in a subspace spanned by all the propagating waveguide modes[25] and, in a later conference paper,[27] studied the contribution of evanescent

[a]Electronic mail: hao.dong@univ-lemans.fr

modes to the maximum directivity, but only for the axial direction at a high frequency. In this case, they found that the inclusion of evanescent modes does not induce any improvement in the directivity.

In this work, we use a similar approach to determine the maximum directivity of acoustic flanged open-ended waveguides while avoiding the POA. We propose a rigorous and algebraic solution to the global maximum directivity factor, applicable to any cross section shape, frequency, and direction. The directivity maximization in the propagating subspace is explored for a three-dimensional circular waveguide and a bidimensional waveguide. Then we synthesize the optimal radiation pattern by multimodal incident waves or an array of point sources within the waveguide. We derive algebraic and well-conditioned solutions for these sound sources and compare the theoretical and synthesized beams. To further demonstrate the optimality of the synthesized beam, we compare it with a cluster of Gaussian shaded modes radiated from the waveguide. Finally, we show that it is reasonable to discard the evanescent modes in the maximization process for designing a hollow waveguide, but the cause is not as explained for the electromagnetic aperture.[27] It is instead related to the radiation efficiency and practical feasibility of the optimum aperture velocity distribution.

II. FORMULATIONS AND THEORETICAL OPTIMAL PATTERNS

A. Modal directivity function

We present a modal formulation of the far-field directivity of an aperture with arbitrary shape mounted in an infinite rigid baffle, as illustrated in Fig. 1. Throughout the paper, we consider time-harmonic linear sound propagation with a time dependence $e^{-i\omega t}$. For simplicity, the following parameters are transformed to be dimensionless: spatial dimensions, including the wavelength, are normalized by a typical dimension parameter of the aperture, the particle velocity $\boldsymbol{v}$ normalized by the speed of sound c, and the sound pressure p normalized by $\rho_0 c^2$, where ρ_0 is the density of air. The sound pressure radiated from the aperture can be expressed by Rayleigh's diffraction formula (Neumann type),[18]

$$p(\boldsymbol{r}) = -ik \int\int_S v_z(x', y', 0) \frac{e^{ik|\boldsymbol{r}-\boldsymbol{r}'|}}{2\pi|\boldsymbol{r}-\boldsymbol{r}'|} dx'dy', \tag{1}$$

where k is the wavenumber, v_z is the normal velocity distribution on S, and $\boldsymbol{r}' = (x', y', 0)$. In the far field, Eq. (1) is approximated by its leading-order term[28]

$$p(r, \theta, \phi) = -ikD(\theta, \phi) \frac{e^{ikr}}{r}, \tag{2}$$

where $D(\theta, \phi)$ is the directivity function,

$$D(\theta, \phi) = \frac{1}{2\pi} \int\int_S v_z(x', y', 0) e^{-i(k_x x' + k_y y')} dx'dy', \tag{3}$$

with $k_x = k \sin\theta \cos\phi$ and $k_y = k \sin\theta \sin\phi$. Equation (3) relates the two-dimensional Fourier transform, or angular spectrum,[28] of the aperture velocity to the far-field radiation.

To couple the radiated field with the propagation within the waveguide, we project the aperture velocity on a complete set of rigid waveguide modes as $v_z(x, y, 0) = \sum_{n=0}^{\infty} v_n \varphi_n(x, y)$.[29,30] $\{\varphi_n\}$ are the Neumann eigenfunctions, solutions of $(\nabla_\perp^2 + \gamma_n^2)\varphi_n = 0$ in S, where $\nabla_\perp^2$ is the transverse Laplacian and $\gamma_n \in \mathbb{R}$ the transverse wavenumbers. They also satisfy the orthogonality $\langle \varphi_n, \varphi_m \rangle = \delta_{nm}$, with the inner product defined as $\langle f, g \rangle \equiv \int\int_S f^* g dS$. Substituting this modal expansion into Eq. (3) yields $D(\theta, \phi) = \sum_{n=0}^{\infty} v_n \Upsilon_n(\theta, \phi)$, where $\Upsilon_n(\theta, \phi) = (1/2\pi)\langle \varphi_n, e^{-i\boldsymbol{k}_\perp \cdot \boldsymbol{x}} \rangle$ is the modal directivity function, with $\boldsymbol{x} = (x, y)$, and $\boldsymbol{k}_\perp = (k_x, k_y)$ the components of the wave vector in the xy plane.

We note a general property regarding the contribution of each mode to the axial radiation ($\theta = 0$). For the fundamental mode $\varphi_0 = 1/\sqrt{S}$ with $\gamma_0 = 0$, it follows that $\Upsilon_0(0, 0) = 1/(2\pi\sqrt{S})$, whereas for all the higher-order modes, $\Upsilon_n(0, 0) = (1/2\pi)\langle \varphi_n, 1 \rangle = 0$. Since only the piston mode contributes to the axial radiation, it is a reasonable guess for the optimum velocity function for the axial maximum directivity.

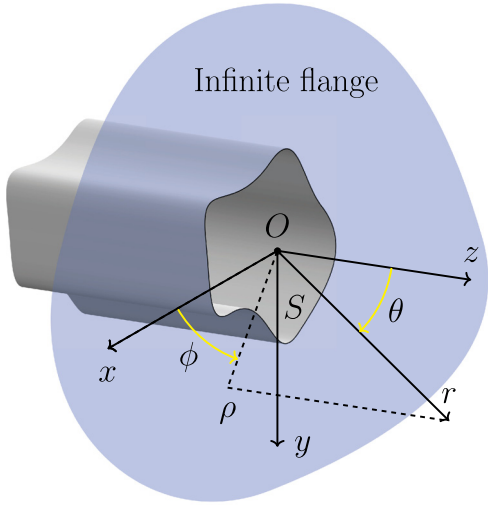

FIG. 1. (Color online) Coordinate system used to formulate sound radiation from a flanged aperture S, assumed to be the opening of a semi-infinite waveguide. The radius vector $\boldsymbol{r}$ is denoted by (x, y, z) or (r, θ, ϕ).

B. Maximum directivity factor

The modal expansions of the velocity and directivity function can be, respectively, written in matrix form as $v_z = \mathbf{v}^T \boldsymbol{\varphi}$ and $D = \mathbf{v}^T \Upsilon$ with column vectors $\mathbf{v} \equiv (v_n)$, $\boldsymbol{\varphi} \equiv (\varphi_n)$, and $\Upsilon \equiv (\Upsilon_n)$. In the far field, the radial velocity can be derived as $v_r = ((ikr - 1)/ikr)p$ from Eq. (2). The radial intensity is then $I_r(r, \theta, \phi) = \frac{1}{2}|p|^2$ and can be rewritten in matrix form as

$$I_r = \frac{k^2}{2r^2} \mathbf{v}^\dagger \mathsf{A}^* \mathbf{v}, \tag{4}$$

https://doi.org/10.1121/10.0020052

where the matrix $\mathsf{A} = \Upsilon\Upsilon^{\dagger}$ is Hermitian and of rank one. It also follows that A is semi-positive definite as $I_r \geq 0$ for all $\mathbf{v} \neq \mathbf{0}$.

The total radiated power W can then be calculated as $W = \int_0^{2\pi} \mathrm{d}\phi \int_0^{\pi/2} I_r(r,\theta,\phi) r^2 \sin\theta \mathrm{d}\theta$ and written in matrix form,

$$W = \frac{k^2}{2}\mathbf{v}^{\dagger}\mathsf{C}^{*}\mathbf{v}, \tag{5}$$

with the Hermitian matrix

$$\mathsf{C} = \int_0^{2\pi} \mathrm{d}\phi \int_0^{\pi/2} \Upsilon\Upsilon^{\dagger} \sin\theta \mathrm{d}\theta \tag{6}$$

being positive definite because $W > 0$ for all $\mathbf{v} \neq \mathbf{0}$. In the literature, C was termed the coupling matrix.[31,32]

Next, we demonstrate that C is strictly real through an alternative derivation of the radiated power. Indeed, it can also be calculated by integrating the normal intensity over the aperture,

$$W = \int\!\!\int_S \frac{1}{2}\mathrm{Re}(pv^{*})\mathrm{d}S = \frac{1}{2}\mathrm{Re}\left(\mathbf{v}^{\dagger}\mathsf{Z}_{\mathrm{r}}^{\dagger}\mathbf{v}\right), \tag{7}$$

where Z_{r} is the radiation impedance matrix defined by $Z_{\mathrm{r},nm} = \langle \varphi_m, \zeta\varphi_n \rangle$, with the linear operator ζ such that $p = \zeta v_z$ given by Eq. (1). Z_{r} being symmetric, Eq. (7) is simplified to

$$W = \frac{1}{2}\mathbf{v}^{\dagger}\mathsf{R}_{\mathrm{r}}\mathbf{v} \tag{8}$$

with $\mathsf{R}_{\mathrm{r}} = \mathrm{Re}(\mathsf{Z}_{\mathrm{r}})$ the radiation resistance. Comparing Eqs. (5) and (8) gives

$$\mathsf{C} = \frac{1}{k^2}\mathsf{R}_{\mathrm{r}}. \tag{9}$$

Therefore, C is real and non-singular. It should be noted that the identity (9) is a discrete form of an operator-form identity derived by Cunefare and Currey.[31] In addition, when restricted to the plane wave mode, this identity, $R_{\mathrm{r},00} = k^2 C_{\mathrm{r},00}$, is exactly the Bouwkamp's impedance theorem[4,33] for a flanged vibrating piston. Equation (9) can, hence, be regarded as the generalized Bouwkamp's impedance theorem for flanged sources with an arbitrary velocity distribution. We also note that the coupling matrix C becomes diagonalized when employing the POA.[25]

The directivity factor is defined as the ratio of the intensity in a specified direction to the intensity that would be produced at the same position by a point source radiating the same power,[4]

$$Q(\theta,\phi) = \frac{I_r(r,\theta,\phi)}{W/2\pi r^2}. \tag{10}$$

Here, we assume the point source is radiated into the half space. Substituting Eqs. (4) and (5) into Eq. (10) yields

$$Q(\theta,\phi) = 2\pi\frac{\mathbf{v}^{\dagger}\mathsf{A}^{*}(\theta,\phi)\mathbf{v}}{\mathbf{v}^{\dagger}\mathsf{C}\mathbf{v}}. \tag{11}$$

The properties of matrices A and C guarantee that Eq. (11) is a generalized Rayleigh quotient.[34] Therefore, Q has a global maximum $Q_{\max}$ that is equal to $2\pi\lambda_{\max}$, where $\lambda_{\max}$ is the largest eigenvalue of the generalized eigenvalue problem

$$\mathsf{A}^{*}\mathbf{v} = \lambda\mathsf{C}\mathbf{v}, \tag{12}$$

and the eigenvector $\mathbf{v}_{\mathrm{opt}}$ corresponding to $\lambda_{\max}$ represents the optimum aperture velocity function $v_{\mathrm{opt}}(x,y) = \mathbf{v}_{\mathrm{opt}}^{\mathrm{T}}\boldsymbol{\varphi}(x,y)$. Equation (12) has only one positive eigenvalue. This can be proved by transforming the generalized eigenvalue problem into a normal one through the Cholesky decomposition $\mathsf{C} = \mathsf{Q}^{\mathrm{T}}\mathsf{Q}$, where Q is a non-singular, real, upper triangle matrix. Let $\mathbf{x} = \mathsf{Q}\mathbf{v}$, and then Eq. (12) becomes

$$\mathsf{Q}^{-\mathrm{T}}\mathsf{A}^{*}\mathsf{Q}^{-1}\mathbf{x} = \lambda\mathbf{x}, \tag{13}$$

where $\mathsf{Q}^{-\mathrm{T}}\mathsf{A}^{*}\mathsf{Q}^{-1}$ is a rank-one, semi-positive definite Hermitian matrix. Therefore, except for its maximum eigenvalue $\lambda_{\max} > 0$, all the other eigenvalues are zeros.

Solving the optimum velocity in the complete space of square integrable functions necessitates incorporation of an infinite number of modes, but in fact, the maximization can only be performed in a finite-dimensional modal subspace. We will show that a reasonable choice of the subspace is the one consisting of all propagating modes ($\gamma_n \leq k$) at a given frequency and that there is no need to incorporate a large number of evanescent modes into the maximization in view of practicality. Even before specific analyses, one could expect good potential of the propagating subspace for generating a directional beam at high frequencies, since its dimension increases with frequency. The effect of including evanescent modes in the maximization will be inspected in Sec. IV B. In the following, we illustrate the theoretical maximum directivity obtained within the propagating subspace in the context of a circular cylindrical waveguide and a bidimensional waveguide.

C. Case study: Circular waveguide

We consider a circular waveguide and take the origin at the center of its opening. We choose the duct radius as the normalization constant. Denote the transverse modes as φ_{mn} and the modal directivity functions as $\Upsilon_{mn} = (1/2\pi)\langle \varphi_{mn}, \mathrm{e}^{-\mathrm{i}\boldsymbol{k}_{\perp}\cdot\boldsymbol{x}} \rangle$, with subscripts $m \in \mathbb{Z}$ the azimuthal order and $n \in \mathbb{N}$ the radial order (see supplementary material[35] for explicit expressions). The two-dimensional Fourier transform in Eq. (3) is now expressed in terms of the radial wavenumber $k_\rho = ||\boldsymbol{k}_{\perp}|| = k\sin\theta$ and the azimuthal angle ϕ. Before solving the maximum directivity factor, we briefly recall the radiation characteristics of the modes (see Baddour *et al.*[14] for thorough discussions). Figures 2(a) and 2(b) show the magnitude spectra of φ_{mn} as a function of k_ρ for the first few modes with $m = 0$ and $m = 2$. The spectra

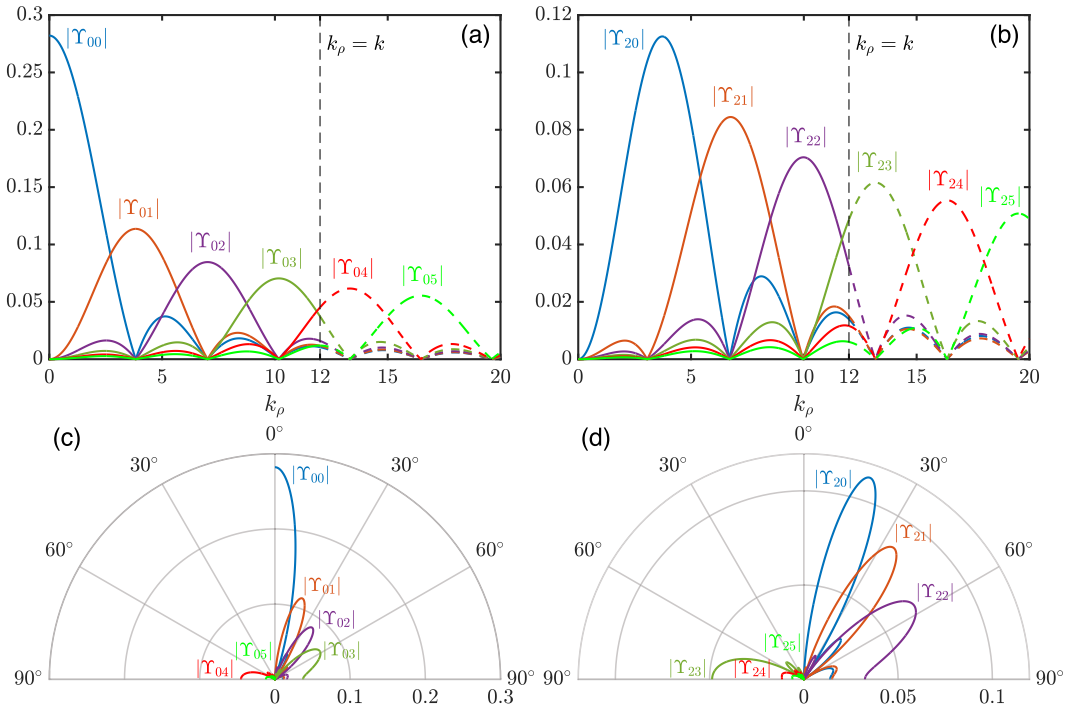

FIG. 2. (Color online) [(a) and (b)] Angular spectra of the first few modes for $m = 0$ and $m = 2$, respectively. The dashed line partitions the spectra into radiating (solid line) and non-radiating (dashed line) components. [(c) and (d)] Corresponding modal directivity patterns as a function of θ at $k = 12$, with cuton and cutoff modes on either side of the 0° axis.

are partitioned into radiating and non-radiating components by the wavenumber k (exemplified by $k = 12$ in the figures). The radiating spectrum for $k_\rho \le k$ is mapped into the far-field directivity function through $\theta = \sin^{-1}(k_\rho/k)$, as shown in Figs. 2(c) and 2(d). For clarity, we plot these axisymmetric patterns in a quadrant and separate the propagating and evanescent modes on either side of the 0° axis. First, it is shown that both propagating and evanescent modes radiate to the far field, but radiation of the cutoff modes is much weaker and is concentrated near the sideline directions ($\theta = 90°$). Second, the general properties mentioned in Sec. II A are manifested: Only the piston mode radiates into the axial direction. In addition, we can observe alternating maxima and minima in the spectrum, which determine the orientation of the main and side lobes.

For a desired direction (θ_d, ϕ_d), the maximum directivity factor Q_{max} is solved in the propagating subspace. The matrix $\mathsf{A} = \Upsilon\Upsilon^\dagger$ is evaluated at (θ_d, ϕ_d); the coupling matrix $\mathsf{C}(k)$ can be calculated from Eq. (6) or through the Bouwkamp's impedance theorem, Eq. (9) (see Zorumski[20] and supplementary material[35] for the radiation impedance matrix). Note that the evaluation of matrix C by numerical integration at many frequencies is time-consuming. We use an alternative multimodal approach[17] to facilitate efficient computation of the radiation impedance matrix by using the PML (see supplementary material[35] for parameters used for computation). More than this, as will be shown in Sec. III, this approach is also used for visualization of the sound field near the aperture.

Let us now investigate the optimal beam patterns for the on-axis ($\theta_d = 0$) and off-axis directions ($\theta_d \ne 0$). As mentioned above, the piston mode φ_{00} is a reasonable guess for the optimum velocity for $\theta_d = 0$. The axial directivity factor of a vibrating piston Q_{pis} can be calculated by substituting $\mathbf{v} = [1, 0, 0, \ldots]^T$ into Eq. (11),

$$Q_{pis} = \frac{k^2}{2 - 2J_1(2k)/k}. \tag{14}$$

Figure 3(a) compares $Q_{max}(0)$ with Q_{pis}. It is shown that Q_{pis} almost reaches the theoretical maximum value. Note that Q_{max} jumps to a value slightly higher than Q_{pis} when passing through the cutoff wavenumbers, which is due to the participation of a new cuton mode and is related to the Wood's anomalies.[36] For $\theta_d = 0$, only the axisymmetric modes contribute to the optimal pattern, so the jumps only occur at γ_{0n}. Figure 3(b) shows the optimum directivity patterns in the xz plane at several frequencies. Note that for a circular electromagnetic radiating aperture, the directivity factor from a uniform electric field, $Q_{uni} = (2\pi/\lambda)^2$, is regarded as the highest attainable value, although it is obtained under both the POA and transverse electromagnetic assumption.[26] Polo-López *et al.*[25,27] verify that the maximum directivity factor indeed cannot exceed Q_{uni}, regardless of whether the evanescent modes are included. In the acoustic case, however, we show that Q_{pis}, without any approximation, is not unsurpassed, especially if the evanescent modes are taken into account (see Sec. IV B); even $Q_{max} \gg Q_{pis}$ is possible.

Realizing off-axis optimal beams necessitates a more sophisticated arrangement of modes with orders $m \ne 0$. Note that due to rotational symmetry, the maximum

https://doi.org/10.1121/10.0020052

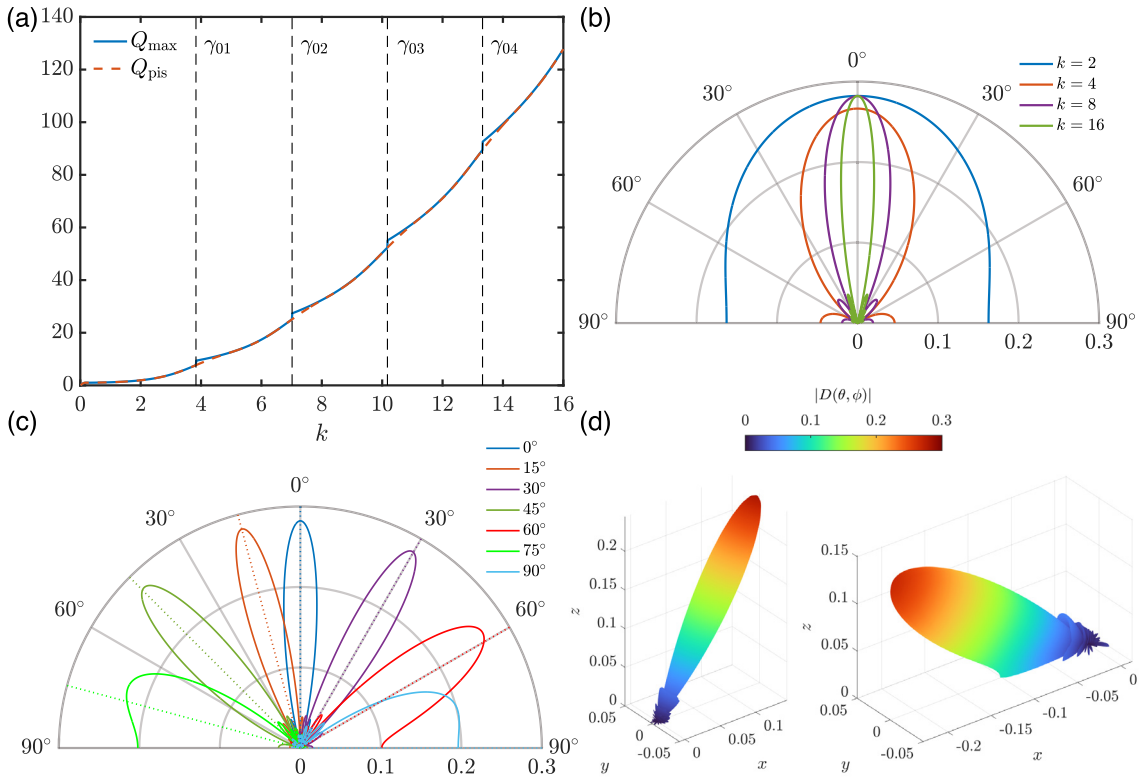

FIG. 3. (Color online) (a) Comparison of $Q_{\max}(0)$ and Q_{pis} as a function of frequency. (b) Optimum directivity patterns for $\theta_{\text{d}} = 0°$ in the xz plane at several frequencies. (c) Optimum directivity patterns in the xz plane at $k = 16$ for different target θ_{d} marked with dotted lines. For clarity, the figure shows patterns for either $\phi_{\text{d}} = 0°$ (for $\theta_{\text{d}} = 0°$, 30°, 60°, and 90°) or $\phi_{\text{d}} = 180°$ (for $\theta_{\text{d}} = 15°$, 45°, and 75°). (d) Three-dimensional optimum patterns steered to directions $(30°, 0°)$ and $(60°, 180°)$ at $k = 16$. In (b)–(d), $||\mathbf{v}_{\text{opt}}|| = 1$.

directivity factor is independent of the azimuthal angle ϕ_{d}. Changing ϕ_{d} simply results in a rotation of the optimal beam pattern about the z axis. Figures 3(c) and 3(d) show the optimum directivity patterns obtained at $k = 16$ for several θ_{d}. It is shown that the optimal beam becomes more directional as it is steered from the sideline to the axial direction. Moreover, for small off-axis angles, the beam is steered precisely to the desired direction, and its mainlobe exhibits good symmetry; in contrast, near the sideline directions, the mainlobe slightly deviates from the target angle, with its symmetry degraded as well. As will be shown in Sec. IV B, participation of the evanescent modes allows precise beam steering into these extreme directions.

D. Case study: Bidimensional waveguide

Since analyzing two-dimensional wave propagation often brings simplification without loss of physical insights, we also study the directivity maximization for a bidimensional waveguide. The geometry is illustrated in Fig. 4. We choose the duct height as the normalization constant. The problem simulates a baffled strip radiator. The directivity is now indicated by the angle θ. Similar to the three-dimensional case, we may derive the matrix-form far-field directivity factor,

$$Q(\theta) = \pi \frac{\mathbf{v}^{\dagger} \mathsf{A}^{*}(\theta) \mathbf{v}}{\mathbf{v}^{\dagger} \mathsf{C} \mathbf{v}}, \tag{15}$$

where the matrices $\mathsf{A} = \Upsilon \Upsilon^{\dagger}$ and $\mathsf{C} = \int_{-\pi/2}^{\pi/2} \mathsf{A}(\theta) \mathrm{d}\theta$. Similarly, we can derive the generalized Bouwkamp's impedance theorem that relates C with R_{r},

$$\mathsf{C} = \frac{2\pi}{k} \mathsf{R}_{\text{r}}. \tag{16}$$

We refer the reader to supplementary material[35] for the above derivations, closed-form expressions of the radiation

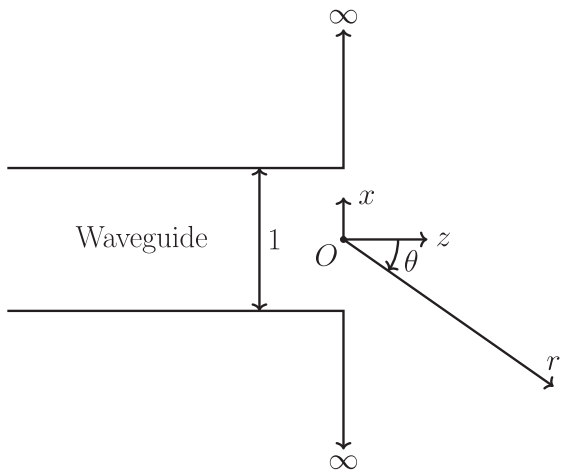

FIG. 4. A bidimensional flanged open-ended waveguide and its coordinate system.

impedances, and a discussion on the identity (16). We point out that unlike the circular aperture, the identity (16) does not obviously hold and cannot be easily proved, e.g., by a trivial change of variables. In turn, an infinite number of integral identities are deduced from it.

In terms of solving the maximum directivity, again, for fast numerical computation, the radiation impedances are computed with the PML-multimodal method.[17] The characteristics of the modal directivity functions and results of the theoretical optimal beams are also presented in the supplementary material[35] for reference.

III. SYNTHESIS OF OPTIMAL PATTERNS

A. Synthesis with incident waves

We present an algebraic expression of a group of incident modes that would synthesize the theoretical optimum directivity pattern. Suppose that the directivity factor in Eq. (11) has been maximized in a subspace spanned by all propagating modes at a given frequency. The resulting vector $\mathbf{v}_{\text{opt}}$, of length N_{p}, gives then the propagating components of the aperture velocity, and one looks for the incident pressure field $\mathbf{p}_+$ that gives rise to this modal content of the propagating velocity field.

Given the incident pressure field $\mathbf{p}_+$ at the output ($z=0$), the total velocity field is

$$\begin{bmatrix} \mathbf{v}_{\text{opt}} \\ \mathbf{v}_{\text{e}} \end{bmatrix} = \mathsf{Y}_{\text{c}}(\mathsf{I}-\mathsf{R})\mathbf{p}_+, \tag{17}$$

where Y_{c} is the characteristic admittance matrix, which is diagonal with elements $\sqrt{k^2-\gamma_n^2}/k$,

$$\mathsf{R} = (\mathsf{I}+\mathsf{Z}_{\text{r}}\mathsf{Y}_{\text{c}})^{-1}(\mathsf{Z}_{\text{r}}\mathsf{Y}_{\text{c}}-\mathsf{I}) \tag{18}$$

is the reflection matrix, and $\mathbf{v}_{\text{e}}$ is the evanescent velocity field (truncated at length N_{e} for computation). By blocking matrices Y_{c} and $(\mathsf{I}-\mathsf{R})$ according to the dimensions of $\mathbf{v}_{\text{opt}}$ and $\mathbf{v}_{\text{e}}$, Eq. (17) can be rewritten as

$$\begin{bmatrix} \mathbf{v}_{\text{opt}} \\ \mathbf{v}_{\text{e}} \end{bmatrix} = \begin{bmatrix} \mathsf{Y}_{\text{c},1} & \mathsf{O} \\ \mathsf{O} & \mathsf{Y}_{\text{c},2} \end{bmatrix} \begin{bmatrix} \mathsf{B}_1 & \mathsf{B}_2 \\ \mathsf{B}_3 & \mathsf{B}_4 \end{bmatrix} \begin{bmatrix} \hat{\mathbf{p}}_+ \\ \mathbf{0} \end{bmatrix}, \tag{19}$$

where $\hat{\mathbf{p}}_+$ represents the first N_{p} components of $\mathbf{p}_+$ (the evanescent components of the incident field are assumed to be zero at the output). The unknowns $\hat{\mathbf{p}}_+$ and $\mathbf{v}_{\text{e}}$ can then be solved as

$$\hat{\mathbf{p}}_+ = \mathsf{B}_1^{-1}\mathsf{Y}_{\text{c},1}^{-1}\mathbf{v}_{\text{opt}} \tag{20}$$

and

$$\mathbf{v}_{\text{e}} = \mathsf{Y}_{\text{c},2}\mathsf{B}_3\hat{\mathbf{p}}_+. \tag{21}$$

As the incoming waves comprise only the propagating modes, the energy flux in the waveguide can be decomposed into right-going and left-going components, from which we can evaluate the transmission efficiency of the directional system,[37]

$$t_W = 1 - \frac{\text{Re}\left(\mathbf{p}_-^{\dagger}\mathsf{Y}_{\text{c}}\mathbf{p}_-\right)}{\text{Re}\left(\mathbf{p}_+^{\dagger}\mathsf{Y}_{\text{c}}\mathbf{p}_+\right)}. \tag{22}$$

We present the synthesis results of the circular waveguide. The optimum velocity $\mathbf{v}_{\text{opt}}$ is first grouped by the azimuthal order m so that Eqs. (20) and (21) are solved for each individual order. In the computation, the total number of modes in the waveguide is $N_{\text{p}}+N_{\text{e}}=20$ for each m, which guarantees $N_{\text{e}} \geq 15$ for any m throughout our considered frequency range $k \leq 16$. The evanescent field in the vicinity of the aperture will cause deviation from the theoretical results. We inspect the differences between the theoretical and synthesized directivity factors as well as the corresponding directivity patterns. The total velocity field $v = v_{\text{opt}} + v_{\text{e}}$ is substituted into Eq. (11) to calculate the synthesized directivity factor $Q_{\text{syn}}(\theta_{\text{d}}, \phi_{\text{d}})$. The results are shown in Figs. 5(a) and 5(b). We have verified that the numerical errors of the PML-multimodal method in both Q_{syn} and $Q_{\max}$ due to the truncation of the modal series are negligible compared to the physical discrepancies $|Q_{\text{syn}} - Q_{\max}|$ shown in Fig. 5(a). The theoretical maximum directivity factor has been realized by incident modes with good agreement. The synthesized pressure field near the opening for $(\theta_{\text{d}}, \phi_{\text{d}}) = (30^\circ, 0^\circ)$ at $k=16$ is shown in Fig. 5(c), exhibiting a directional beam with a near-planar wavefront and emission of many regularly distributed sidelobes. The results suggest that by only maximizing the directivity factor, a regular beam pattern can be generated and synthesized with incident propagating modes. In this sense, our study has provided physically achievable benchmark radiation patterns that can be used as design objectives for aperture antennas.

The transmission coefficients t_W of the incident modes for different target directions are inspected in Fig. 6. Except for the dips near the cutoff wavenumbers due to strong scattering, the power transmission is globally high, indicating good radiation capacity of the directional system.

Radiation pattern synthesis for a bidimensional waveguide can be realized and analyzed in a similar way. The results are briefly presented in the supplementary material.[35]

B. Synthesis with point sources

From a practical point of view, it is meaningful to investigate the radiation pattern synthesis by a realizable source inside the waveguide such as an array of point sources, rather than the more theoretical multimodal incident wave. For simplicity, this problem is studied in the bidimensional case. The synthesis problem is stated as finding a configuration of an array of point sources in the semi-infinite waveguide, including the number, locations, and source strengths, to reconstruct the incident modal amplitudes $\hat{\mathbf{p}}_+$ at the open end given by Eq. (20). The solution is not unique; therefore, to restrict the problem, we consider a

https://doi.org/10.1121/10.0020052

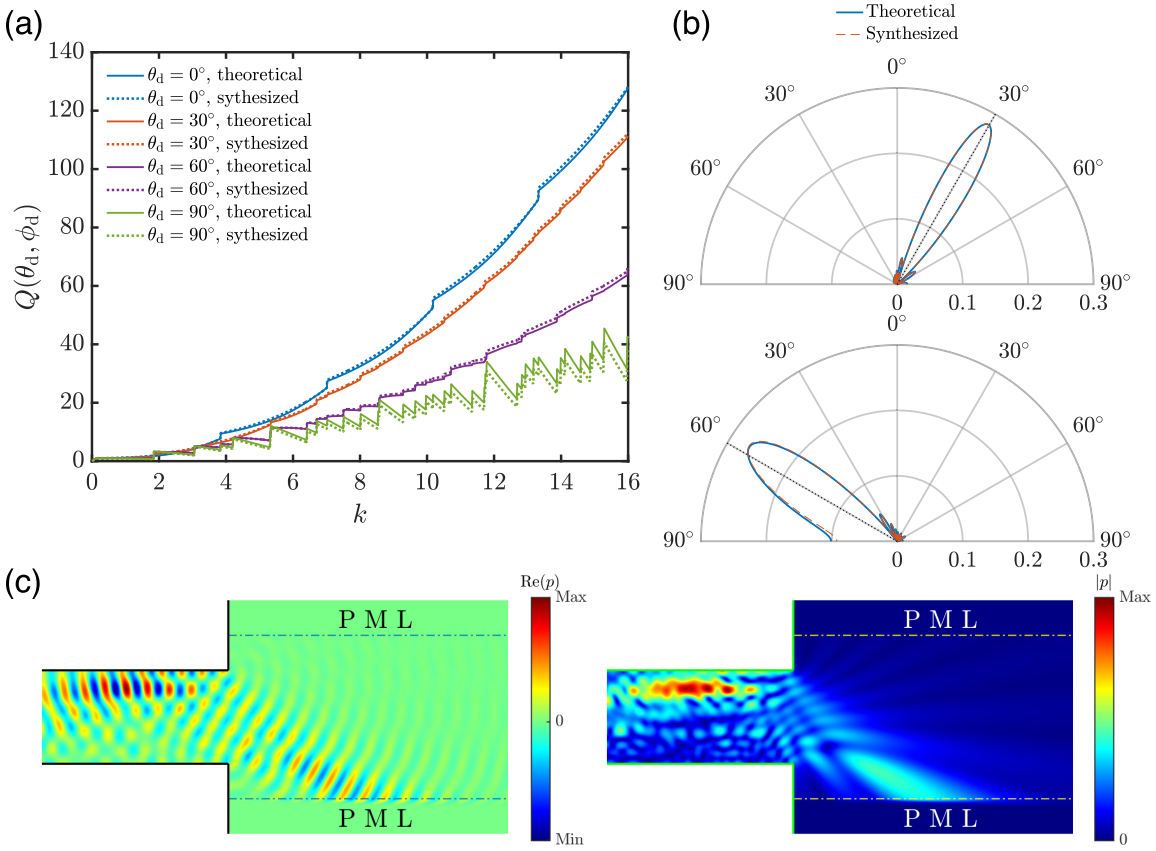

FIG. 5. (Color online) Results of beam pattern synthesis for a circular waveguide. (a) Comparison of the Q_{max} and Q_{syn} for different θ_d. (b) Comparison of the theoretical and synthesized patterns for $(30°, 0°)$ and $(60°, 180°)$ at $k = 16$ in xz plane [corresponding to Fig. 3(c)]. (c) Real part (left) and magnitude (right) of the pressure field in the xz plane generated by incident propagating modes for the directivity synthesis in $(30°, 0°)$ at $k = 16$, computed by the PML-multimodal method. In (b) and (c), $||\mathbf{v}_{opt}|| = 1$.

linear arrangement of point sources located on a transversal line upstream from the opening, far enough to ensure that all the evanescent waves emitted by the sources are negligible at the opening. From the modal representation of the Green's function in the waveguide, we can express $\hat{p}_{+,n}$ in terms of the contribution from M point sources,

$$\sum_{m=0}^{M-1} kQ_m \frac{\varphi_n(x_m)}{-2ik_{z,n}} e^{ik_{z,n}|z_s|} = \hat{p}_{+,n}, \quad 0 \le n \le N_p - 1, \tag{23}$$

where $k_{z,n} = \sqrt{k^2 - \gamma_n^2}$ is the axial wavenumber, and (x_m, z_s) and Q_m are, respectively, the coordinates and strength (complex) of the mth source. Equation (23) can be rewritten in matrix form,

$$\mathsf{E}\mathbf{q} = \mathbf{c}, \tag{24}$$

where $E_{nm} = \varphi_n(x_m)$, $c_n = -2ik_{z,n}\hat{p}_{+,n}e^{-ik_{z,n}|z_s|}/k$, and $\mathbf{q} = (Q_n)$. Let $M = N_p$, and equally space the sources on the transversal line, that is, let $x_m = -\frac{1}{2} + (m/(N_p - 1))$ for $0 \le m \le N_p - 1$, and then the linear algebraic equation has a unique solution $\mathbf{q} = \mathsf{E}^{-1}\mathbf{c}$. More importantly, the condition number of the matrix E is well controlled with such arrangement, even for a high dimension (see supplementary material[35] for the condition number analysis).

The field emitted by the point sources (before being scattered by the opening) is then given by

$$p(x, z) = \sum_{m=0}^{M-1} \sum_{n=0}^{\infty} kQ_m \frac{\varphi_n(x_m)}{-2ik_{z,n}} e^{ik_{z,n}|z - z_s|}, \tag{25}$$

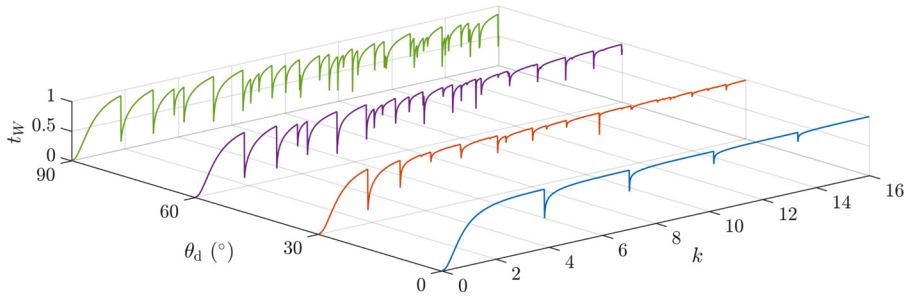

FIG. 6. (Color online) Transmission efficiency of the incident waves that synthesize optimal beams in different directions.

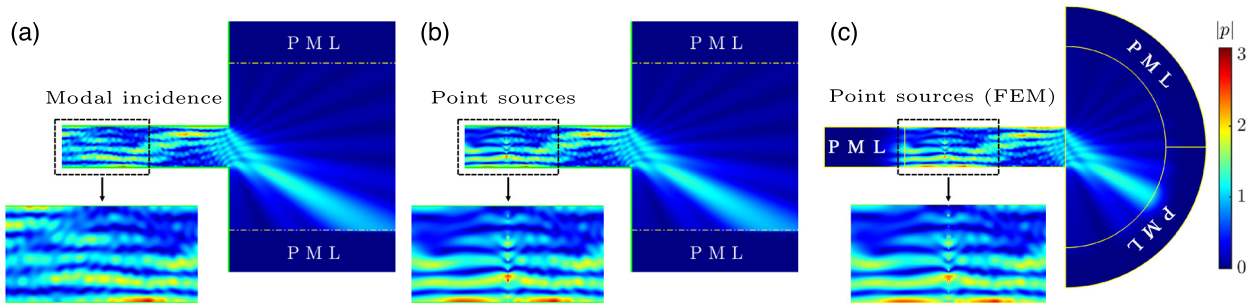

FIG. 7. (Color online) Pressure field near the opening of a bidimensional waveguide for beam pattern synthesis. $\theta_d = 30^\circ$ at $k = 30$. (a) Synthesis with multimodal incidence, $||\mathbf{p}_+|| = 1$; (b) synthesis with point sources; (c) FEM validation of (b).

which incorporates evanescent waves near the sources, and the number of modes is truncated at 30 for computation at our studied frequency ($k = 30$, $N_p = 10$). For verification purpose, the results have been validated by the finite element method (FEM), using (x_m, z_s, Q_m) as model inputs (Fig. 7 and Mm. 1).

Mm. 1. Beam steering achieved by a point-source array in a bidimensional waveguide at $k = 30$.

IV. TWO COMMENTS ON THE OPTIMALITY

A. Comparison with Gaussian shaded modes

In this section, we introduce an alternative method for creating a directional beam via a cluster of Gaussian shaded modes and compare it with our proposed synthesized beam (multimodal incidence) within the framework of a bidimensional waveguide. A group of Gaussian shaded modes propagating in the waveguide shows ray-like behavior at high frequencies.[38,39] As illustrated in Fig. 8, the beam is propagating at an angle $\theta_0 = \sin^{-1}(n_0\pi/k)$ with respect to the z axis, where n_0 is the order of its central mode. Letting its propagation trajectory pass through the origin, we intuitively create a directional beam steered to the θ_0 direction. Its modal amplitudes can be obtained by weighting those of the Green's function in the waveguide by a Gaussian window centered at the n_0th mode,[38,39]

$$p_n(z) = \frac{\varphi_n(x_s)}{-2ik_{z,n}} e^{ik_{z,n}|z-z_s|} e^{-(n-n_0)^2/2\sigma^2}, \tag{26}$$

where (x_s, z_s) are coordinates of the point source, and σ is the standard deviation of the Gaussian distribution. For comparison with the synthesized beam, in this study, only the propagating modes are used to construct the beam ($0 \le n \le N_p - 1$). Equation (26) describes an incident field consisting of two beams directed at angles $\pm\theta_0$. A single beam can be obtained by placing the source on one of the walls. After emitting from the source, it is reflected between the walls N_r times before the aperture diffraction. Figure 8 shows the case of $N_r = 1$, where the source coordinates can be determined from the geometrical relations.

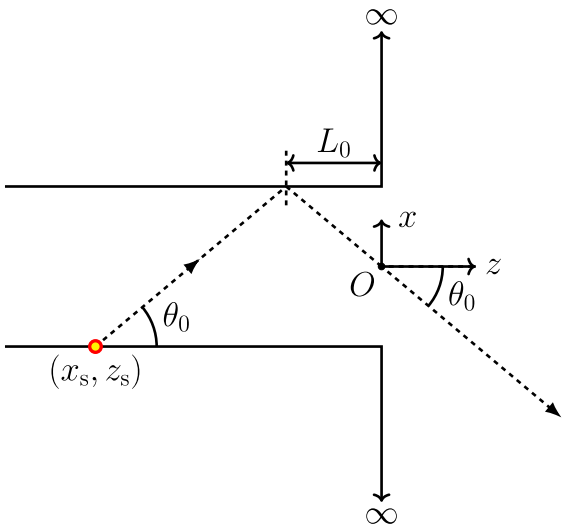

FIG. 8. (Color online) Schematic diagram of the propagation trajectory and source location for intuitively building a directional beam. $x_s = \frac{1}{2}(-1)^{N_r}$, $z_s = -(2N_r + 1)L_0$, and $L_0 = \frac{1}{2}\cot\theta_0$.

For a given center mode n_0, the directivity factor of the Gaussian shaded modes targeted at angle θ_0 is dependent on the number of reflections N_r and the standard deviation σ. An optimal beam with the highest directivity factor is then obtained by solving a two-parameter optimization problem. Figure 9(a) compares the directivity factor of the synthesized beam (by modal incidence) with that of the optimized Gaussian shaded modes for $1 \le n_0 \le N_p - 1$. Note that in the case of $n_0 = 0$ (thus, $\theta_0 = 0$), the beam is not well-defined since $z_s \to -\infty$. It is clear that the Gaussian shaded modes do not allow continuous beam steering, and as expected, at these discrete steering angles, the beam is always less directional than the synthesized beam. Nevertheless, the variation of its directivity factor follows closely that of the synthesized beam. Figure 9(b) compares their sound fields at $k = 30$ for $n_0 = 4$ ($\theta_0 = 24.8^\circ$), with the source location for the optimized Gaussian shaded modes ($N_r = 0$, $\sigma = 0.90$) and the trajectory marked out. The near field and sidelobes of the synthesized modes display more regular pattern than the Gaussian shaded modes, which might account for the higher directivity.

https://doi.org/10.1121/10.0020052

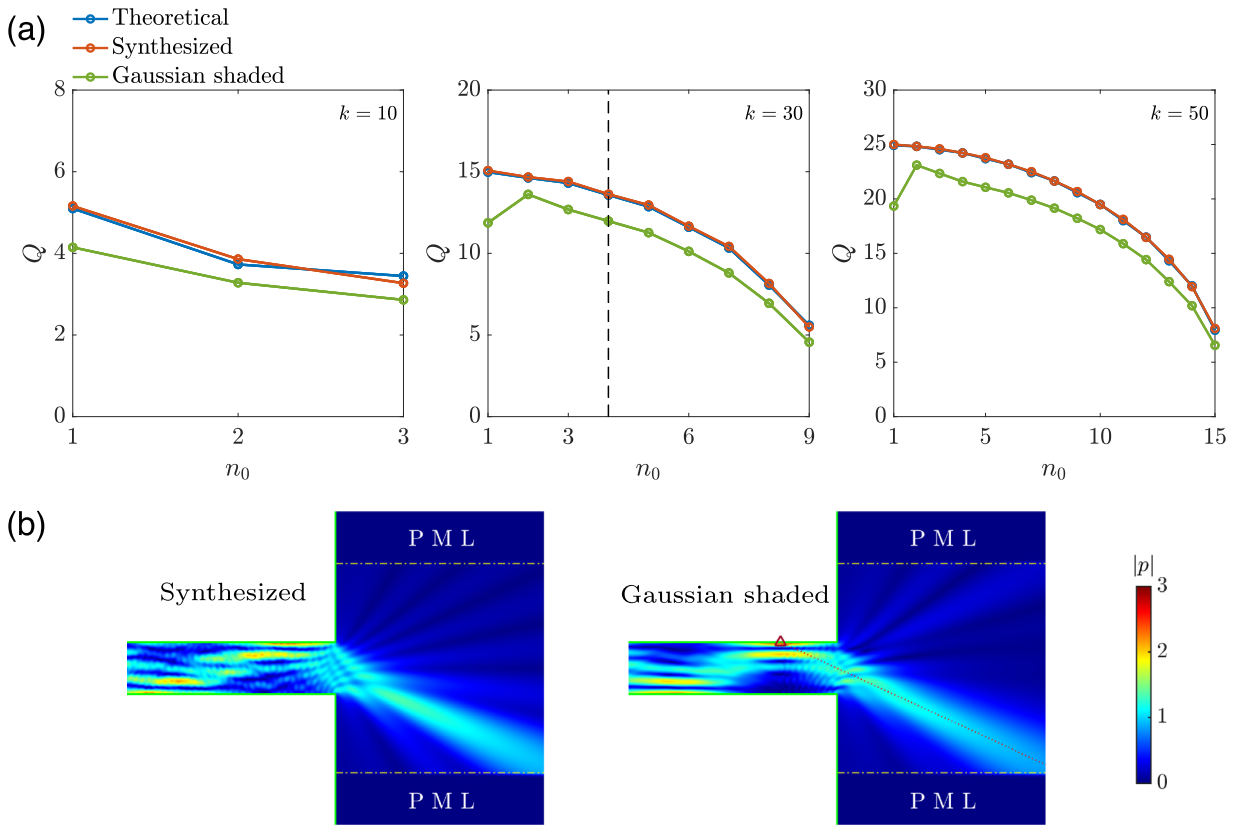

FIG. 9. (Color online) (a) Comparison of the directivity factors of the optimized Gaussian shaded modes for $\theta_0 = \sin^{-1}(n_0\pi/k)$ and the theoretical and synthesized (by modal incidence) directivity factors in θ_0 in a bidimensional waveguide. (b) Comparison of the magnitude pressure field between the synthesized beam ($Q = 13.6$) and the Gaussian shaded modes ($Q = 12.0$) at $k = 30$, for $n_0 = 4$, $\theta_0 = 24.8°$, corresponding to the dashed line in (a). $||\mathbf{p}_+||$=1.

B. Effect of evanescent modes

In this section, we inspect the influence of evanescent modes on the directivity maximization problem. We recall the definition of the radiation efficiency of a given velocity distribution $v(x, y)$ on a surface S,[19,28,40]

$$\tau = \frac{W}{\frac{1}{2}\int\int_S |v(x,y)|^2 \mathrm{d}S}, \tag{27}$$

where W is the actual radiated power given by Eq. (8), and the denominator is an assumed reference power, defined as the power radiated by a portion S of an infinite planar piston vibrating with the root-mean-square (rms) value of the actual velocity on S. Equation (27) can be simplified as

$$\tau = \mathbf{v}^\dagger \mathsf{R}_\mathrm{r} \mathbf{v} \tag{28}$$

by normalization such that $||\mathbf{v}|| = 1$. Equation (28) indicates that the radiation efficiency of each individual mode is given by the corresponding diagonal element of the radiation resistance matrix. The radiation efficiency of an evanescent mode is much lower than a propagating mode.[19]

By solving the maximization problem in a subspace spanned by all propagating modes and at least one evanescent mode, we examine the variations of the maximum directivity factor $Q_{\max}$, radiation efficiency τ of the optimum velocity, and the proportion of evanescent components in the velocity $||\mathbf{v}_\mathrm{e}||^2/||\mathbf{v}_\mathrm{opt}||^2$ as a function of N_e. Without loss of generality, we study the bidimensional aperture and present the results in Fig. 10(a). The participation of evanescent modes results in an elevation of $Q_{\max}$, particularly at lower frequencies, where $Q_{\max}$ in the axial direction can significantly surpass Q_{pis}. Moreover, the results show a significant decrease in the radiation efficiency accompanied by a rapid increase in the proportion of evanescent components, even for small values of N_e. According to Eq. (27), a decrease in efficiency corresponds to a lower radiated power for a given rms velocity. Figure 10(b) exemplifies the optimum directivity patterns for $N_\mathrm{e} \leq 3$ (plotted for $||\mathbf{v}_\mathrm{opt}|| = 1$). As the sound intensity $I_r(r, \theta) \propto |D(\theta)|^2$ at given radial distance and frequency, a decrease in the radiated power is manifested by the "shrinking" of the directivity pattern.

An aperture velocity distribution dominated by evanescent modes can be difficult to implement in hollow waveguides. Even if it is possible, the system is likely inefficient. In contrast, in Sec. III, we have demonstrated that the optimum velocity obtained in the propagating subspace is physically achievable and exhibits good transmission efficiency. Therefore, for traditional hollow horn antennas, it is reasonable to maximize the directivity in the propagating subspace and use the results for design. Nevertheless, in some cases with $N_\mathrm{e} \geq 1$, the efficiency still remains at a practical level. For example, as shown in Fig. 10(b), $\theta_\mathrm{d} = 90°$ case, the

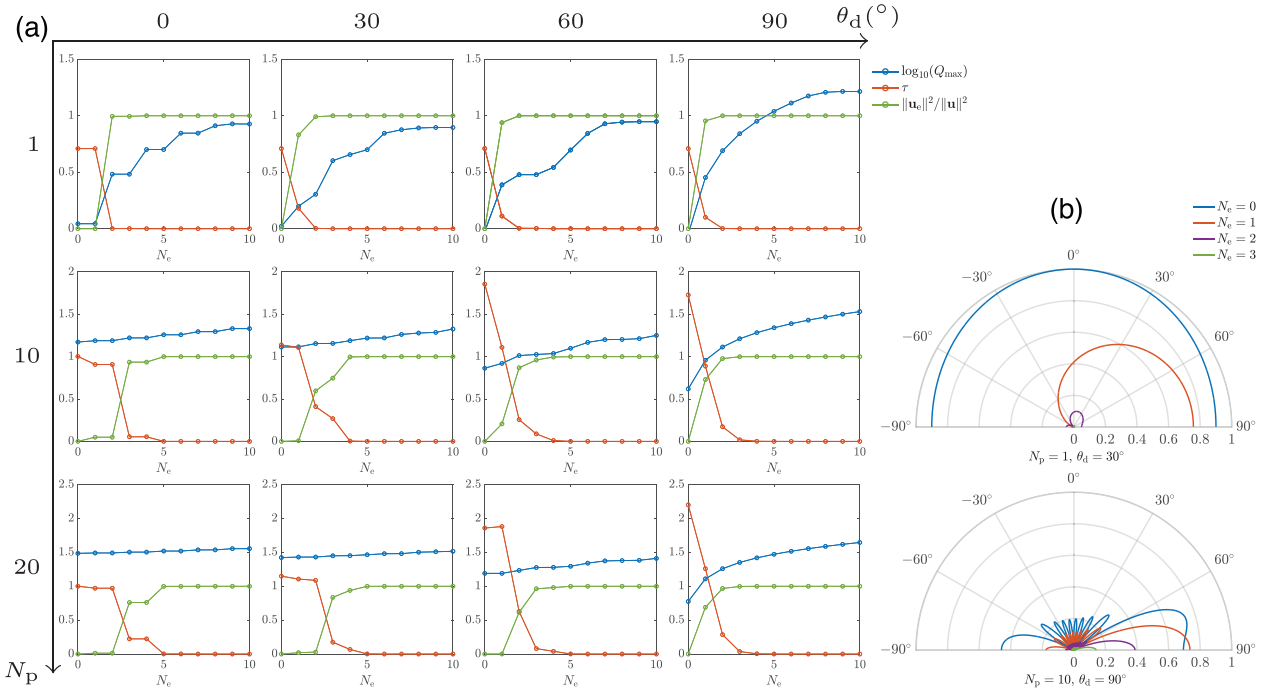

FIG. 10. (Color online) (a) Dependence of $\log_{10}(Q_{max})$, τ, and $||\mathbf{v}_e||^2/||\mathbf{v}_{opt}||^2$ on N_e at $k = 0.5\pi$ ($N_p = 1$), 9.5π ($N_p = 10$), and 19.5π ($N_p = 20$) for different target directions. (b) Typical optimum directivity patterns for incremental N_e. The bidimensional aperture is studied.

assistance of the first evanescent mode (orange line) does not significantly reduce the efficiency compared to $N_e = 0$ (blue line) but in turn steers the mainlobe precisely into the desired sideline direction. According to Fig. 10(a), the optimal velocity for $N_e = 1$ is dominated by its evanescent components with a weight factor of 0.73. It could be achieved when the waveguide is filled with structured media through which evanescent modes can be effectively emitted.

Figure 10(a) shows that the increase in Q_{max} with N_e slows down for smaller angles and higher frequencies. The previous work on the electromagnetic aperture[27] only studied the case of $\theta_d = 0$ at a high frequency ($N_p = 77$), and the results showed a trend of convergence similar to the present case of $\theta_d = 0$, $N_p = 20$, showing limited contribution of the evanescent modes. However, our analysis reveals more complicated reasoning for discarding them in the maximization. It will be relevant in the future to conduct similar comprehensive analysis for the electromagnetic aperture.

We also note that any orthogonal basis defined on aperture surface can be used for the directivity maximization, and the aforementioned properties of the solution will not be affected by such a choice. Indeed, projecting the transverse Laplacian with the boundary condition onto an orthogonal basis always leads to propagating and evanescent modes. The use of rigid waveguide modes is more suited for coupling the propagation models in horns.[37,41]

V. CONCLUSION

The directivity factor of a flanged planar source, i.e., an aperture or a solid vibrating surface, has been formulated as a generalized Rayleigh quotient, which guarantees a global maximum in a given modal subspace. Using the transverse modes of a rigid waveguide as the expansion basis, an important finding is the formation of the radiation-efficient and -inefficient optimum velocity distributions depending on whether the evanescent modes are included in the maximization. It is reasonable to benchmark a hollow waveguide antenna design against an optimal pattern obtained in the propagating subspace. The theoretical pattern can be effectively synthesized by a group of incident modes or a point-source array within the waveguide, and these directional systems exhibit good transmission properties. When the velocity subspace is enlarged with the evanescent modes, the maximized directivity factor increases at the expense of radiation efficiency, and the optimum velocity will be dominated by its evanescent components. As a result, it is not practical to realize these patterns via hollow waveguides. However, the evanescent modes are crucial for precise beam steering in extreme directions. These patterns could be achieved if the waveguide is designed by filling structured media near its opening. In addition, we have derived rigorous integral expressions of the multimodal radiation impedances for a flanged bidimensional waveguide. An infinite number of integral identities are deduced from the generalized Bouwkamp's impedance theorem.

The present fundamental theory has provided benchmark directivity factors and patterns for subsequent explorations of structure design, such as horn antenna design by shape optimization[41] or filling metamaterials.[23] The formulations are also applicable to unflanged waveguides, subject to the evaluation of free-field modal directivity functions.

https://doi.org/10.1121/10.0020052

ACKNOWLEDGMENTS

This work was partly funded by Le Mans Acoustique in the framework of the Pays de la Loire region. The authors declare that they have no conflicts to disclose. The data that support the findings of this study are available from the corresponding author upon reasonable request.

[1]D. B. Keele, Jr. "Effective performance of Bessel arrays," J. Audio Eng. Soc. **38**(10), 723–748 (1990).
[2]B. Rafaely, "Spherical loudspeaker array for local active control of sound," J. Acoust. Soc. Am. **125**(5), 3006–3017 (2009).
[3]P. J. Westervelt, "Parametric acoustic array," J. Acoust. Soc. Am. **35**(4), 535–537 (1963).
[4]L. Beranek and T. Mellow, *Acoustics: Sound Fields, Transducers and Vibration*, 2nd ed. (Academic, London, 2019), pp. 190, 463–510, 690–691.
[5]Y. Xie, W. Wang, H. Chen, A. Konneker, B.-I. Popa, and S. A. Cummer, "Wavefront modulation and subwavelength diffractive acoustics with an acoustic metasurface," Nat. Commun. **5**(1), 5553 (2014).
[6]L. Zhao, E. Laredo, O. Ryan, A. Yazdkhasti, H.-T. Kim, R. Ganye, T. Horiuchi, and M. Yu, "Ultrasound beam steering with flattened acoustic metamaterial Luneburg lens," Appl. Phys. Lett. **116**(7), 071902 (2020).
[7]E. E. Altshuler and D. S. Linden, "Wire-antenna designs using genetic algorithms," IEEE Antennas Propag. Mag. **39**(2), 33–43 (1997).
[8]R. Pritchard, "Maximum directivity index of a linear point array," J. Acoust. Soc. Am. **26**(6), 1034–1039 (1954).
[9]J. L. Butler and S. L. Ehrlich, "Superdirective spherical radiator," J. Acoust. Soc. Am. **61**(6), 1427–1431 (1977).
[10]H. Levine and J. Schwinger, "On the radiation of sound from an unflanged circular pipe," Phys. Rev. **73**(4), 383–406 (1948).
[11]G. Homicz and J. Lordi, "A note on the radiative directivity patterns of duct acoustic modes," J. Sound Vib. **41**(3), 283–290 (1975).
[12]A. Snakowska, H. Idczak, and B. Bogusz, "Modal analysis of the acoustic field radiated from an unflanged cylindrical duct—Theory and measurement," Acta Acust. united Acust. **82**(2), 201–206 (1996).
[13]G. Gabard and R. Astley, "Theoretical model for sound radiation from annular jet pipes: Far- and near-field solutions," J. Fluid Mech. **549**, 315–341 (2006).
[14]B. Baddour, P. Joseph, A. McAlpine, and R. Leung, "Acoustic radiation characteristics of cutoff modes from ducts," J. Sound Vib. **541**, 117306 (2022).
[15]Y. Nomura, I. Yamamura, and S. Inawashiro, "On the acoustic radiation from a flanged circular pipe," J. Phys. Soc. Jpn. **15**(3), 510–517 (1960).
[16]D. Homentcovschi and R. Bercia, "Re-expansion method for generalized radiation impedance of a circular aperture in an infinite flange," J. Acoust. Soc. Am. **144**(1), 32–40 (2018).
[17]S. Félix, J.-B. Doc, and M. A. Boucher, "Modeling of the multimodal radiation from an open-ended waveguide," J. Acoust. Soc. Am. **143**(6), 3520–3528 (2018).
[18]J. W. S. Rayleigh, *The Theory of Sound* (Dover, New York, 1945), Vol. 2, pp. 487–491.
[19]C. Morfey, "A note on the radiation efficiency of acoustic duct modes," J. Sound Vib. **9**(3), 367–372 (1969).
[20]W. E. Zorumski, "Generalized radiation impedances and reflection coefficients of circular and annular ducts," J. Acoust. Soc. Am. **54**(6), 1667–1673 (1973).
[21]J. Kemp, D. Campbell, and N. Amir, "Multimodal radiation impedance of a rectangular duct terminated in an infinite baffle," Acta Acust. united Acust. **87**(1), 11–15 (2001).
[22]E. R. Geddes, "On the use of the Hankel transform for sound radiation," in *Proceedings of Audio Engineering Society Convention 93*, San Francisco (October 1–4, 1992).
[23]X. Chen, H. Feng Ma, X. Ying Zou, W. Xiang Jiang, and T. Jun Cui, "Three-dimensional broadband and high-directivity lens antenna made of metamaterials," J. Appl. Phys. **110**(4), 044904 (2011).
[24]B. N. Nagarkar and R. Finch, "Sinusoidal horns," J. Acoust. Soc. Am. **50**(1A), 23–31 (1971).
[25]L. Polo-López, J. Córcoles, J. A. Ruiz-Cruz, J. R. Montejo-Garai, and J. M. Rebollar, "On the theoretical maximum directivity of a radiating aperture from modal field expansions," IEEE Trans. Antennas Propag. **67**(4), 2781–2786 (2019).
[26]W. L. Stutzman and G. A. Thiele, *Antenna Theory and Design*, 3rd ed. (Wiley, New York, 2012), pp. 349–351, 361–362.
[27]L. Polo-López, J. Córcoles, and J. A. Ruiz-Cruz, "Contribution of the evanescent modes to the power radiated by an aperture," in *Proceedings of the 2021 IEEE MTT-S International Microwave Symposium (IMS)*, Atlanta, GA (June 7–25, 2021), pp. 474–477.
[28]E. G. Williams, *Fourier Acoustics: Sound Radiation and Nearfield Acoustical Holography* (Academic, London, 1999), pp. 15–55.
[29]P. M. Morse and K. U. Ingard, *Theoretical Acoustics* (McGraw-Hill, New York, 1968), pp. 492–522.
[30]A. D. Pierce, *Acoustics: An Introduction to Its Physical Principles and Applications*, 3rd ed. (Springer Nature, Cham, Switzerland, 2019).
[31]K. A. Cunefare and M. N. Currey, "On the exterior acoustic radiation modes of structures," J. Acoust. Soc. Am. **96**(4), 2302–2312 (1994).
[32]M. N. Currey and K. A. Cunefare, "The radiation modes of baffled finite plates," J. Acoust. Soc. Am. **98**(3), 1570–1580 (1995).
[33]C. Bouwkamp, "A contribution to the theory of acoustic radiation," Philips Res. Rep. **1**(4), 251–277 (1946).
[34]R. A. Horn and C. R. Johnson, *Matrix Analysis*, 2nd ed. (Cambridge University, New York, 2012).
[35]See supplementary material at https://doi.org/10.1121/10.0020052 for further details on formulations of the circular waveguide regarding the transverse modes, generalized radiation impedances, and parameters used for implementing the PML-multimodal method; formulations of the bidimensional waveguide regarding the transverse modes, directivity factor, generalized radiation impedances, and perfectly matched layer (PML)-multimodal method; the results of the directivity maximization and radiation pattern synthesis; and condition number analysis of the transfer matrix.
[36]R. W. Wood, "XLII. On a remarkable case of uneven distribution of light in a diffraction grating spectrum," London, Edinburgh Dublin Philosoph. Mag. J. Sci. **4**(21), 396–402 (1902).
[37]V. Pagneux, N. Amir, and J. Kergomard, "A study of wave propagation in varying cross-section waveguides by modal decomposition. Part I. Theory and validation," J. Acoust. Soc. Am. **100**(4), 2034–2048 (1996).
[38]A. Kamel and L. B. Felsen, "On the ray equivalent of a group of modes," J. Acoust. Soc. Am. **71**(6), 1445–1452 (1982).
[39]S. Félix and V. Pagneux, "Ray-wave correspondence in bent waveguides," Wave Motion **41**(4), 339–355 (2005).
[40]K. A. Cunefare, "The minimum multimodal radiation efficiency of baffled finite beams," J. Acoust. Soc. Am. **90**(5), 2521–2529 (1991).
[41]H. Dong, H. Gao, X. Feng, and Y. Shen, "Shape optimization of acoustic horns for improved directivity control and radiation efficiency based on the multimodal method," J. Acoust. Soc. Am. **149**(3), 1411–1424 (2021).